Exponentially Expanded Grid Network Approach (EEGNA): An Efficient Way for the Simulation of Stiff Electrochemical Problems

DENG, Zhao-Xiang(邓兆祥) LIN, Xiang-Qin* (林祥钦) TONG, Zhong-Hua(童中华)
Department of Chemistry, University of Science and Technology of China, Hefei, Anhui 230026, China

The exponentially expanded space grid was incorporated into the network approach to overcome the problem of low simulation efficiency during the simulations of electrochemical problems with stiff kinetics or wide dispersion of diffusion coefficients, resulting in an effective electrochemical simulation method: exponentially expanded grid network approach (EEGNA). The stability and accuracy of the EEGNA for the simulation of various electrode processes coupled with different types of homogeneous reactions were investigated.

Keywords electrochemical simulation, exponentially expanded grid network approach, stiff problem

Introduction

The method using electric network model to describe electrochemical reaction-diffusion process on the basis of the theory of network thermodynamics[1-4] is termed a network approach.[5] Network thermodynamics is a marriage of classical and non-equilibrium thermodynamics along with network theory and kinetics to provide a practical framework for handling the systems that are highly structured and interactive, and thus can not be reduced to simple components without losing a great deal of their system identity.[4] The heart of the network approach is to spatially discretize non-stationary or stationary reaction-diffusion equations through finite difference approximation, whereas keeping the time variable continuous. Therefore, the parabolic partial differential equations (PDEs) representing the electrochemical problems under specific boundary and initial conditions could be transformed into coupled linear or nonlinear ordinary differential equations (ODEs), which can be expressed into trapezoidal electrical networks.[4,5] Since the network response could be solved by electronic simulators such as SPICE or PSPICE (personal computer simulation program with integrated circuit emphasis), no sophisticated mathematics are involved during the simulation process. The network approach substantially simplifies the simulations of various physical and chemical problems, and thus wide applications have been found not only in electrochemistry but also in other areas such as colloidal science.[6-13]

Early work on network simulation mainly was concentrated on uniform grid network approach (UGNA).[5,14] During the simulation of systems with wide range of diffusion coefficients or coupled with fast homogeneous chemical reactions, UGNA is impractically time-consuming and thus becomes hopeless. In more recent publications,[15] non-uniform grid technique was attempted. The basic idea of this non-uniform grid technique (quasi-uniform grid network approach-QUGNA) is to use different grid thicknesses for the species with different diffusion coefficients or different homogeneous kinetic constants. However, for systems with non-overlapping diffusion or reaction layers, this non-uniform network model will need hundreds of space grids in order to obtain an accurate simulation. Therefore, the computation speed can not be improved too much by QUGNA even for small systems. In addition, the major part of this kind of non-uniform network model has to be frequently reconstructed when different systems are considered.

Our previous investigations have shown that truly non-uniform grid (such as exponentially expanded grid) technique could be used in the network simulation of a simple electron transfer process coupled with *iR* drop distortion or surface adsorption of electroactive species.[16,17] We herein try to demonstrate that the major difficulties of the network approach in dealing with stiff problems or widely dispersed diffusion coefficients of interesting species could be successfully overcome by introducing exponentially expanded space grids into the network approach.

Theory

Mass transport model

As for semi-infinite linear diffusion, mass transport of substances is governed by Fick's second law:

* E-mail: xqlin@ustc.edu.cn
Received September 17, 2002; revised March 3, 2003; accepted May 2, 2003.
Project supported by the Chinese Academy of Sciences (No. 9002kj951-A1-507) and the National Natural Science Foundation of China (No. 20173054).

$$\frac{\partial c}{\partial t} = D\frac{\partial^2 c}{\partial x^2} \tag{1}$$

where t, x and c are physical quantities representing time, distance and concentration, respectively. Under semi-infinite condition, diffusion could be considered to happen only within a finite thickness $[6(D\tau)^{1/2}]$ of solution layer, where τ is the total experimental time. Eq. (1) can be approximated as the following ODEs by using finite difference discretization on the spatial variable x.

$$\frac{\partial c}{\partial t}\Delta x/D^{1/2} = \Delta[\frac{\Delta c}{\Delta x/D^{1/2}}] \tag{2}$$

Eq. (2) could be expressed in the form of an electric network model as seen in Fig. 1, which is a trapezoidal network constituted by linear electric components such as resistors and capacitors. The electric tensions and currents in this network correspond to the concentrations and fluxes of species in the diffusion layer.

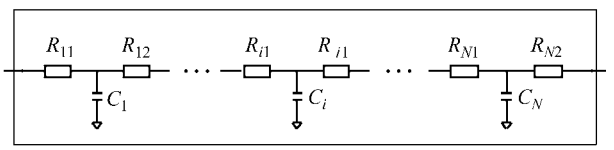

Fig. 1 Electric network model representing a linear diffusion process.

For exponentially expanded network model, the resistances and capacitances are defined by the following equations:

$$R_{i1} = \frac{\Delta x/D^{1/2}}{e^{\beta}-1}\cdot[e^{\beta(i-0.5)} - e^{\beta(i-1)}] \tag{3}$$

$$R_{i2} = \frac{\Delta x/D^{1/2}}{e^{\beta}-1}\cdot[e^{\beta i} - e^{\beta(i-0.5)}] \tag{4}$$

$$C_i = \Delta x/D^{1/2}e^{\beta(i-1)} \tag{5}$$

where, i = 1, 2, …, N;

$$\Delta x = \frac{6(e^{\beta}-1)}{e^{N\beta}-1}(D\tau)^{1/2} \tag{6}$$

Considering a system containing species with different diffusion coefficients, and the maximum and minimum diffusion coefficients are denoted as D_{max} and D_{min}. Assuming at least 10 exponentially expanding grids are needed for accurate description of a diffusion layer (the validity of this assumption will be shown later), Eq. (7) is obtained based on Eq. (6).

$$\Delta x = \frac{6(e^{\beta}-1)}{e^{10\beta}-1}(D_{min}\tau)^{1/2} = \frac{6(e^{\beta}-1)}{e^{N\beta}-1}(D_{max}\tau)^{1/2} \tag{7}$$

Rearrangement of Eq. (7) gives:

$$\frac{D_{max}}{D_{min}} = \left(\frac{e^{N\beta}-1}{e^{10\beta}-1}\right)^2 \tag{8}$$

From Eq. (8), it can be seen that the range of D_{max}/D_{min} could be as wide as $[2.2326\times10^4, 1]$ for $N = 20$, $\beta = 0.5$; and $[4.852\times10^8, 1]$ for $N = 20$, $\beta = 1$. Therefore the EEGNA has an outstanding advantage on the UGNA and QUGN in dealing with systems with extremely large variation of diffusion coefficients.[5,14,15]

For systems coupled with first-order irreversible following homogeneous reaction, the solution layer (reaction layer) containing the electrode reaction product is extremely thin, and needs very fine space division. This could correspond to thousands or even tens of thousands of simulation grids in the case of the uniform grid network approach, leading to impractical simulation speed and memory usage. Although the QUGNA partially circumvents this difficulty, it still need several hundreds of grids in order to achieve an accurate simulation.[14,15]

Considering the following first order homogeneous chemical reaction

$$A \xrightarrow{k_1} B \tag{9}$$

The corresponding reaction layer thickness is usually expressed as $\mu = (D/k_1)^{1/2}$, and at least five grids must be comprised in this reaction layer for a simulation with satisfying accuracy, *i.e.*, the following relationship must hold

$$\Delta x = \frac{6(e^{0.5}-1)}{e^{N\beta}-1}(D\tau)^{1/2} \leqslant \mu/5 = \frac{(D/k_1)^{1/2}}{5} \tag{10}$$

Rearrangement of Eq. (10) gives

$$k_1^* = k_1\tau \leqslant [\frac{e^{N\beta}-1}{30(e^{\beta}-1)}]^2 \tag{11}$$

where k_1^* is the dimensionless form of the first order kinetic rate constant k_1. The maximum value of k_1^* that an exponentially expanded network model (EEGNM) can deal with could be estimated from Eq. (11). Table 1 shows that about 10 to 20 network nodes (grids) are enough for treating almost all experimentally achievable systems in the real world,[18,19] which is much more efficient than either UGNA or QUGNA. Test results as shown in Fig. 2 show that 10—30 network grids will take a typical CPU time of less than 3.5 s for a Cleron 667 processor. This time increases almost exponentially with the grid number and will be more than 20 s for 200 grids and more than 140 s for 600 grids. This means that the EEGNA is at least 10—30 times faster than QUGNA or UGNA.

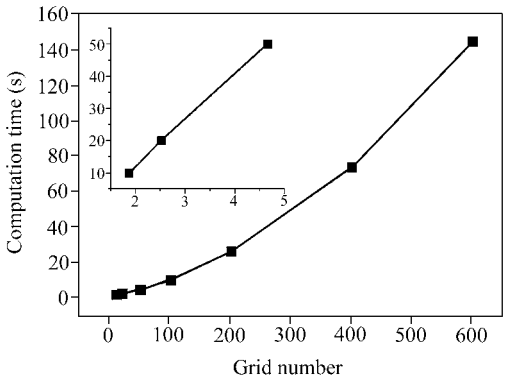

Fig. 2 Relationship between the required computation time and the grid number used in a typical network simulation.

Table 1 Upper limit of k_1^* for an exponentially expanded grid network model (EEGNM)

N	β	k_1^*
10	0.5	5.737×10^1
	1	1.826×10^5
15	0.5	8.621×10^3
	1	4.022×10^9
20	0.5	1.281×10^6
	1	8.858×10^{13}

Cyclic voltammetric problems

For the following electrode process,

$$\mathrm{B} \longrightarrow \mathrm{A} \quad (k_1) \tag{12-1}$$

$$\mathrm{A} + \mathrm{e} \leftrightarrow \mathrm{B} \quad (k^0, E^0) \tag{12-2}$$

$$\gamma\mathrm{B} \leftrightarrow \mathrm{C} \quad (k_2, k_{-2}, K_2 = k_2/k_{-2}) \tag{12-3}$$

$$\mathrm{C} \leftrightarrow \gamma\mathrm{A} \quad (k_3, k_{-3}, K_3 = k_3/k_{-3}) \tag{12-4}$$

the mass transport of Ox and Red are governed by the following PDEs,

$$\frac{\partial c_\mathrm{A}}{\partial t} = D_\mathrm{A}\frac{\partial^2 c_\mathrm{A}}{\partial x^2} + k_1 c_\mathrm{B} + \gamma k_3 c_\mathrm{C} - \gamma k_{-3} c_\mathrm{A}^\gamma \tag{13-1}$$

$$\frac{\partial c_\mathrm{B}}{\partial t} = D_\mathrm{B}\frac{\partial^2 c_\mathrm{B}}{\partial x^2} - k_1 c_\mathrm{B} - \gamma k_2 c_\mathrm{B}^\gamma + \gamma k_{-2} c_\mathrm{C} \tag{13-2}$$

$$\frac{\partial c_\mathrm{C}}{\partial t} = D_\mathrm{C}\frac{\partial^2 c_\mathrm{C}}{\partial x^2} + k_2 c_\mathrm{B}^\gamma + k_{-3} c_\mathrm{A}^\gamma - k_3 c_\mathrm{C} - k_{-2} c_\mathrm{C} \tag{13-3}$$

The boundary conditions are

$$t \geqslant 0 \quad x \to \infty \quad c_j(x,t) = c_j^*,\ j = \mathrm{A}, \mathrm{B}, \mathrm{C} \tag{14}$$

$$f_\mathrm{A}(0,t) = -f_\mathrm{B}(0,t) = [k_\mathrm{f} c_\mathrm{A}(0,t) - k_\mathrm{b} c_\mathrm{B}(0,t)] \tag{15}$$

where t and x have their usual meanings, c_j is the concentration of species "j" (j = A, B or C), and c_j^* is the bulky or initial concentrations.

The electron-transfer kinetics is assumed to obey the Butler-Volmer equations[20] as in Eqs. (16) and (17),

$$k_\mathrm{f} = k^0 \exp[-\alpha F(E - E^0)/(RT)] \tag{16}$$

$$k_\mathrm{b} = k^0 \exp[(1-\alpha) F(E - E^0)/(RT)] \tag{17}$$

with k_f and k_b representing the forward and backward electron-transfer rate constants, k^0 being the standard heterogeneous rate constant, α the electron transfer coefficient (symmetry factor), F the Faradic constant, E the applied potential between the working and reference electrodes, E^0 the formal electrode potential, R the gas constant and T the temperature in Kelvin. The corresponding network model is shown in Fig. 3.

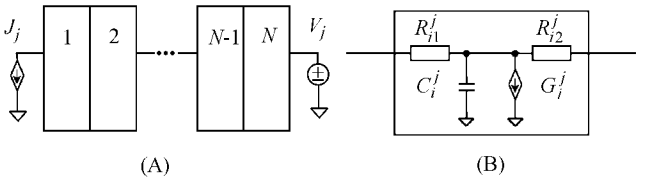

Fig. 3 Network model for species j. j represents species A, B and C. (A) Global network model, (B) the subcircuit in (A).

The definitions of the resistances and capacitances are

$$R_{i1}^j = \frac{\Delta x / D_j^{1/2}}{\mathrm{e}^\beta - 1} \cdot [\mathrm{e}^{\beta(i-0.5)} - \mathrm{e}^{\beta(i-1)}] \tag{18}$$

$$R_{i2}^j = \frac{\Delta x / D_j^{1/2}}{\mathrm{e}^\beta - 1} \cdot [\mathrm{e}^{\beta i} - \mathrm{e}^{\beta(i-0.5)}] \tag{19}$$

$$C_i^j = \Delta x / D_j^{1/2} \mathrm{e}^{\beta(i-1)} \tag{20}$$

$$\Delta x = \frac{6(\mathrm{e}^\beta - 1)}{\mathrm{e}^{N\beta} - 1}(D_{\max}\tau)^{1/2} \tag{21}$$

where $D_{\max}$ is the maximum diffusion coefficient among D_A, D_B and D_C.

G_i^j is a linear or nonlinear voltage-dependent current source (VCCS) defined by

$$G_i^\mathrm{A} = (-k_1 c_\mathrm{B} - \gamma k_3 c_\mathrm{C} + \gamma k_{-3} c_\mathrm{A}^\gamma) C_i^\mathrm{A} \tag{22-1}$$

$$G_i^\mathrm{B} = (k_1 c_\mathrm{B} + \gamma k_2 c_\mathrm{B}^\gamma - \gamma k_{-2} c_\mathrm{C}) C_i^\mathrm{B} \tag{22-2}$$

$$G_i^\mathrm{C} = (-k_2 c_\mathrm{B}^\gamma - k_{-3} c_\mathrm{A}^\gamma + k_3 c_\mathrm{C} + k_{-2} c_\mathrm{C}) CC_i \tag{22-3}$$

where V_j and J_j have the following definitions

$$V_j = c_j^* \tag{23}$$

$$J_A = k_f c_A^0 - k_b c_B^0 \quad (24\text{-}1)$$

$$J_B = -(k_f c_A^0 - k_b c_B^0) = -J_A \quad (24\text{-}2)$$

The capacitors in the diffusion network have initial voltages of

$$IC_j = c_j^* \quad (25)$$

Eq. (12) and the EEGNM in Fig. 3 can represent E, E_i, EC_i, EC_{i2}, CE, CE_i and the catalytic (EC_{cat}) mechanisms when different model parameters as in Table 2 are taken.

Table 2 Model parameters of selected electrochemical mechanisms involving first and second-order chemical reactions

Mechanism	γ	k_1	k_2	k_{-2}	k_3	k_{-3}	k_b
E	—	0	0	0	0	0	$\neq 0$
E_i	—	0	0	0	0	0	0
EC	1	0	$\neq 0$	$\neq 0$	0	0	$\neq 0$
EC_i	1	0	$\neq 0$	0	0	0	$\neq 0$
EC_{i2}	2	0	$\neq 0$	0	0	0	$\neq 0$
CE	1	0	0	0	$\neq 0$	$\neq 0$	$\neq 0$
CE_i	1	0	0	0	$\neq 0$	$\neq 0$	0
EC_{cat}	—	$\neq 0$	0	0	0	0	$\neq 0$

Experimental

Calculations were conducted on an IMB compatible PC with a Pentium 120 MHz processor. A PC with a faster Cleron 667 Porcessor was also used for the investigation of the dependence of the computation time on the number of grids used. A PSPICE 5.0 (DOS Version) or PSPICE 5.1 (Windows based) was used for calculation of the transient responses of the network models designed for specific electrochemical mechanisms. Microcal Origin 5.0 was used for plotting of data. Network models representing different network models were input into PSPICE either using a standard text-based input file or as a graphical schematic file (in PSPICE 5.1). Simulations could then be done immediately after completing input of the models.

Results and discussion

E *and* E_i

The simulation results for a reversible electron-transfer process along with Nicholson and Shain's numerical solutions are presented in Table 3, from which it can be seen that the EEGNA with $N = 10$, and $\beta = 0.5$ or 1.0 is accurate enough for the E case, and the simulation with $\beta = 0.5$ is slightly better than $\beta = 1$. Further researches were conducted to investigate the influence of N on the simulation accuracy. The simulated cyclic voltammograms show that for $\beta = 0.5$, the simulated voltammetric curves become visibly overlapped when $N > 8$, while for $\beta = 1$, the simulation results converged only at $N > 4$. Therefore, $\beta = 1$ is especially efficient for a fast simulation with satisfactory accuracy. It is also noteworthy that more than 100 grids are needed for the UGNA to obtain a similar result.

Table 3 Simulated current functions for a reversible cyclic voltammetric process[a]

$E - E_{1/2}$	Ψ_r^b		
	N.S.[c]	EEGNA	
		$\beta = 0.5$	$\beta = 1.0$
0.120	0.009	0.0092	0.0092
0.080	0.042	0.0417	0.0418
0.040	0.160	0.1606	0.1610
0	0.380	0.3797	0.3804
−0.0285	0.4463	0.4463	0.4468
−0.040	0.438	0.4381	0.4385
−0.080	0.353	0.3531	0.3516
−0.120	0.280	0.2803	0.2776

[a] Simulation parameters: $E_{start} = E_{1/2} + 0.400$ V; potential step, 1 mV; $a = Fv/(RT) = 38.92\ s^{-1}$; $N = 10$. [b] Ψ_r is the current function for a reversible process defined by Nicholson and Shain.[21] [c] N.S. is the numerical results obtained through solving the corresponding integral equations (numerical resolution).[22]

As discussed above, EEGNA can also handle systems with extremely wide dispersion of diffusion coefficients. Based on Eq. (8), the allowed ratio between D_{min} and D_{max} could be as low as 2.061×10^{-9} for $N = 20$ and $\beta = 1$. This is evidenced by the simulation results in Table 4. The simulated peak potentials and peak currents are virtually identical with the results for $D_A = D_B$. Although the predicted limit for D_B/D_A is 2.061×10^{-9}, it can be seen that serious deviation only happens when $D_B/D_A < 2.061 \times 10^{-14}$. The underlying reason for this is that for $\beta = 1$, $N = 4$ is enough to give a simulation with acceptable accuracy, while during the derivation of Eq. (8) we assumed the minimum value of N to be 10. If the mutation happens at $N < 4$, Eq. (8) becomes Eq. (26), and the lower limit for D_B/D_A will be $D_{min}/D_{max} = 1.22 \times 10^{-14}$ for $N = 20$ and $\beta = 1$, consistent with the results in Table 4.

$$\frac{D_{min}}{D_{max}} = \left(\frac{e^{4\beta} - 1}{e^{N\beta} - 1}\right)^2 \quad (26)$$

The above system is electrochemically reversible, and the interfacial electron flowing is determined by the relatively slow diffusion. For a system where the rate of the electron-transfer is only moderate, the electron flux will be dependent on both the diffusion and the heterogeneous electron-transfer. Our simulated results for such systems are listed in Table 5 along with the results from solving corresponding integral equation numerically. The simulated results with $\beta = 0.5$ or 1 are in good consistency with

the integral equation results. The simulated cathodic peak currents for $\beta = 0.5$ and 1 show only 0.04% and 0.1% deviations from the numerical solutions of corresponding integral equation (N.S. results). For anodic peak currents, $\beta = 0.5$ still give results with less than 0.04% deviations from the N.S. results, but for $\beta = 1$ these deviations are about 1%—2%. However, our numerical experiments show that 0.1%—0.2% deviations could be obtained with slightly decreased β value such as 0.9.

Table 4 Simulated peak current functions and peak potentials for reversible voltammetric processes with different ratios between the diffusion coefficients of species B and A[a]

D_B/D_A	$-E_{pc}$ (mV)	Ψ_{pc}	E_{pa} (mV)	$-\Psi_{pa}$
1	28.5	0.4468	29.0	0.3494
2.061×10^{-9}	28.5	0.4468	29.0	0.3494
2.061×10^{-10}	28.5	0.4469	29.5	0.3472
2.016×10^{-11}	28.5	0.4469	29.0	0.3444
2.061×10^{-12}	29.0	0.4468	29.0	0.3431
2.061×10^{-13}	29.0	0.4469	28.5	0.3439
2.061×10^{-14}	29.0	0.4490	29.0	0.3436
2.061×10^{-15}	34.0	0.4765	48.0	0.3140

[a] Simulation parameters: $E_{start} = E^0 + 0.400$ V; $E_{switch} = E^0 - 0.400$ V; $E^0 = 0.00$ V $- (RT/F)\ln(D_B/D_A)^{1/2}$ (using such values of E^0 should, theoretically, always result in simulated cyclic voltammograms with identical shape); potential step, 1 mV; $a = Fv/(RT) = 38.92\ s^{-1}$; $N = 20$, $\beta = 1$. E_{pc} and E_{pa} are cathodic and anodic peak potentials respectively, while Ψ_{pc} and Ψ_{pa} are the corresponding cathodic and anodic peak current functions.

If the electron-transfer rate (assuming Butler-Volmer kinetics) is so slow that the reverse electron-transfer could be ignored within the experimentally accessible potential window, this process is usually defined as an irreversible electrode process. For $N = 10$ the simulated results by EEGNA (Table 6) are accurate for both $\beta = 0.5$ and 1.0. Our research also shows that for UGNA ($\beta = 0$) the simulated dimensionless peak current function only reached 0.4951 for $N = 100$, and 0.4955 for $N = 150$, indicating a low simulation efficiency.

EC_i, EC *and* EC_{i2} *cases*

Just as predicted above, EEGNA is especially advantageous in processing stiff problems. For $N = 20$, $\beta = 1.0$, assuming Nernstian electron-transfer, Eq. (11) gives the upper limit of processable homogeneous rate constant of $8.858\times10^{13}/\tau$, corresponding simulation results were shown in Table 7. For such a rate constant, the results could be identical with the E_i process under appropriate transformations of the potential axis. As seen from Table 7, the simulation result with $\tau = 1.0$ is excellent. Slightly decreasing β to 0.9 and increasing N to 22 could improve the simulation accuracy further. It should be noted that when $N = 20$ and $\beta = 1.0$, $k_2^* = 8.858\times10^{13}$ exactly corresponds to the requirement that five concentration grids are comprised in the reaction layer. However, this restriction is rather conservative, and the simulations are still very accurate even for higher value of k_2^*, *e.g.* 8.858×10^{14} (see Table 7, column C). Further increasing k_2^* to 8.858×10^{15} resulted in severely deteriorated results. These results show that for $N = 20$ and $\beta = 1.0$, EC_i scheme with $k_2^* = 8.858\times10^{13}$—$8.858\times10^{14}$ could be accurately simulated, which actually reaches the upper limit of existing fastest first order chemical reactions.

Table 5 Simulated peak current functions and peak potentials for quasi-reversible electrode reactions with different values of the dimensionless heterogeneous rate constant (Λ)[a]

β	Λ	$-E_{pc}$ (mV)		Ψ_{pc}		E_{pa} (mV)		$-\Psi_{pa}$	
		N.S.		N.S.		N.S.		N.S.	
0.5	1×10^{-2}	258.7	258.9	0.3506	0.3507	250.5	250.1	0.1601	0.1601
	4×10^{-2}	187.6	187.6	0.3518	0.3519	177.5	177.7	0.1969	0.1970
	0.16	117.6	117.7	0.3610	0.3611	107.5	107.6	0.2398	0.2399
	1.28	46.6	46.7	0.4133	0.4134	44.5	44.6	0.3147	0.3147
	12.8	30.6	30.6	0.4421	0.4421	30.5	30.8	0.3430	0.3430
1.0	1×10^{-2}	259.1	258.9	0.3505	0.3507	250.5	250.1	0.1630	0.1601
	4×10^{-2}	187.4	187.6	0.3516	0.3519	178.5	177.7	0.1997	0.1970
	0.16	117.1	117.7	0.3609	0.3611	107.5	107.6	0.2419	0.2399
	1.28	46.6	46.7	0.4137	0.4134	44.5	44.6	0.3169	0.3147
	12.8	31.0	30.6	0.4427	0.4421	30.5	30.8	0.3455	0.3430

[a] Simulation parameters: $E_{start} = E^0 + 0.400$ V; $E_{switch} = E^0 - 0.400$ V; $E^0 = 0.0$ V, $D_A = D_B = 1\times10^{-5}\ cm^2\cdot s^{-1}$; potential step, 1 mV; $a = Fv/(RT) = 38.92\ s^{-1}$; $N = 10$. E_{pc} and E_{pa} are cathodic and anodic peak potentials, respectively, while Ψ_{pc} and Ψ_{pa} are the corresponding cathodic and anodic peak current functions.

Table 6 Simulated current functions for an irreversible cyclic voltammogram[a]

E_{ir}[c] (V)	Ψ_{ir}[b]		
	N.S.	β	
		0.5	1
0.140	0.008	0.008	0.008
0.100	0.035	0.035	0.035
0.060	0.145	0.145	0.145
0.020	0.406	0.406	0.406
−0.0053	0.4958	0.4957	0.4956
−0.020	0.472	0.472	0.472

[a] Simulation parameters: $D_A = D_B = 10^{-5}$ cm²/s, $E_{start} = E^0 + 0.200$ V, $\alpha = 0.5$, $a = 38.92$ s^{-1}, $\Lambda = k^0(D_A a)^{-1/2} = 10^{-4}$, $N = 10$. [b] $\Psi_{ir} = \Psi_r/\alpha^{1/2}$ (see ref. 21). [c] $E_{ir} = \alpha(E - E_0) + (RT/2F)\ln(\pi\alpha/\Lambda^2)$ (see Ref. 21).

Table 7 Simulated cyclic voltammetric current functions for a reversible electron transfer followed by an irreversible first-order chemical reaction[a]

E_{ec}[b] (V)	Ψ_{ir}	Ψ_{ec}			
	N.S.	A	B	C	D
0.140	0.008	0.008	0.008	0.007	0.006
0.100	0.035	0.035	0.035	0.034	0.029
0.060	0.145	0.146	0.145	0.143	0.124
0.020	0.406	0.407	0.406	0.403	0.373
−0.0053	0.4958	0.4959	0.4959	0.4959	0.4960[c]
−0.020	0.472	0.473	0.473	0.473	0.485
−0.070	0.323	0.321	0.323	0.322	0.331

[a] Simulation parameters: $\Lambda = \infty$; $D_A = D_B = 10^{-5}$ cm²·s^{-1}; $E_{start} = E^0 + 0.600$ V; $E_{switch} = E^0 + 0.100$ V; $k_2^* = 8.858 \times 10^{13}$, $N = 20$, $\beta = 1.0$ (A), $N = 22$, $\beta = 0.9$ (B); $k_2^* = 8.858 \times 10^{14}$, $N = 20$, $\beta = 1.0$ (C); $k_2^* = 8.858 \times 10^{15}$, $N = 20$, $\beta = 1.0$ (D). [b] $E_{ec} = E - E^0 - (RT/2F)[-1.56 + \ln(k_2^{\neq})] - 0.0053$ V.[21] [c] Here the simulated peak potential is not −5.3 mV but −10.2 mV.

In the EC process, the following chemical reaction is reversible. For this case, systems with different homogeneous rate constants were simulated by EEGNA, and the results shown in Table 8 indicate that they are in good agreement with Nicholson and Shain's results.

Table 8 Simulated voltammetric peak current functions and peak potentials for a reversible electron transfer followed by a reversible first-order chemical reaction[a]

$K_2\lambda^{-1/2}$	N.S.		$\beta = 1.0$		$\beta = 0.5$	
	E_p	Ψ	E_p	Ψ	E_p	Ψ
0.1	−23.6	0.449	−23.4	0.4485	−22.8	0.4490
0.55	−11.5	0.459	−10.9	0.4579	−11.4	0.4585
2.0	−0.9	0.474	−0.7	0.4719	−0.1	0.4725
10.0	5.5	0.487	6.3	0.4852	5.9	0.4857

[a] Simulation parameters: $\Lambda = \infty$; $D_A = D_B = 10^{-5}$ cm²·s^{-1}; $E_{start} = E^0 + 0.400$ V; $\lambda = (k_2 + k_{-2})/a = 9$; $N = 10$ for $\beta = 1.0$ or $N = 15$ for $\beta = 0.5$.

As for the EC_{i2} scheme, the coupled chemical process is an irreversible dimerization reaction, which is a frequently encountered case in electropolymerizations. Table 9 lists the simulated peak potentials and peak current functions along with the calculated results by Olmstead[23] for different values of k_2. The results with $\beta = 0.5$ seem more accurate than $\beta = 1$, but for $\beta = 1$ only 10 grids are needed and the errors are less than 0.2%.

Table 9 Simulated current functions for a reversible charge transfer followed by an irreversible dimerization reaction[a]

$2k_2c_A^*/a$	Ψ_r[b]		
	Ref.[23]	β	
		0.5	1
0.0050	0.447	0.4465	0.4458
0.0150	0.447	0.4469	0.4462
0.0400	0.448	0.4478	0.4471
0.1000	0.450	0.4499	0.4492
0.2250	0.454	0.4438	0.4532
0.4750	0.461	0.4602	0.4597
1.0000	0.470	0.4698	0.4693
2.7000	0.486	0.4859	0.4855
24.000	0.514	0.5137	0.5135

[a] Simulation parameters: $D_A = D_B = 10^{-5}$ cm²/s, $E_{start} = E^0 + 0.400$ V, $E_{start} = E^0 - 0.300$ V, $a = 38.92$ s^{-1}, potential step, 1 mV; $N = 15$, $\beta = 0.5$ or $N = 10$, $\beta = 1$. [b] Current function for a reversible electron transfer, see ref. 21.

Further investigations were also conducted for extremely large value of k_2. Results in Table 10 exhibit that even for the dimensionless second order rate constant $k_2c_A^*/a$ as large as 5×10^{11}, $\beta = 1$ and $N = 20$ are enough to give satisfactory results.

Table 10 Simulated voltammetric peak current functions and peak potentials for a reversible electron transfer followed by an irreversible dimerization[a]

$2k_2c_A^*/a$	Ref.[23]		This work	
	E_p	Ψ_p	E_p	Ψ_p
1×10^4	52	0.526	52.9	0.5264
1×10^8	131	0.526	130.9	0.5267
1×10^{12}	210	0.526	209.9	0.5267

[a] Simulation parameters: $\Lambda = \infty$; $D_A = D_B = 10^{-5}$ cm²·s^{-1}; $E_{start} = E^0 + 0.400$ V; $a = 38.92$; $N = 20$, $\beta = 1.0$.

CE and CE_i *cases*

Tables 11 and 12 give the simulation results for CE process by EEGNA. From Table 11, it can be seen that the accuracy of EEGNA for the simulation of CE scheme is also very high, and the simulation accuracy is hardly influenced by the value of β. In addition, due to the efficiency of EEGNA in the processing of stiff system, the simulation of CE scheme is also very accurate for systems with very fast preceding chemical reaction (see Table 11) that is actually in equilibrium due to the very high rates of both the forward and backward reactions.

Table 11 Simulated voltammetric peak current functions and half-peak potentials for a reversible chemical reaction preceding a reversible charge transfer[a]

$(K_3\lambda^{1/2})^{-1}$	N.S.		$\beta = 0.5$		$\beta = 1.0$	
	$E_{p/2}'$[b] (mV)	Ψ_{CE}[c]	$E_{p/2}'$ (mV)	Ψ_{CE}	$E_{p/2}'$ (mV)	Ψ_{CE}
0.2	29.3	0.406	29.6	0.4062	29.6	0.4056
1	34.4	0.300	35.0	0.2998	35.0	0.2996
10	62.2	0.079	62.3	0.0789	62.3	0.0789

[a] Simulation parameters: $\Lambda = \infty$; $D_A = D_B = 10^{-5}$ cm^2·s^{-1}; $E_{start} = E^0 + 0.400$ V; $\lambda = (k_3 + k_{-3})/a = 9$; $N = 10$ for $\beta = 1.0$ or $N = 15$ for $\beta = 0.5$. [b] $E_{p/2}' = (E_{p/2} - E^0) - (RT/F)\ln[K_3/(1 + K_3)]$. [c] $\Psi_{CE} = i/FAc^*(D_A a)^{1/2}$, where c^* is the sum of the equilibrium concentrations of species A and C.

Table 12 Simulated voltammetric peak current functions and half-peak potentials for a reversible chemical reaction preceding a reversible charge transfer[a]

λ	N.S.		This work	
	$-E_{p/2}$ (mV)	Ψ_{CE}	$-E_{p/2}$ (mV)	Ψ_{CE}
2.5×10^1	38.8	0.079	38.2	0.07892
2.5×10^3	97.5	0.079	97.1	0.07894
2.5×10^5	156.6	0.079	156.1	0.07896
2.5×10^7	215.8	0.079	215.2	0.07893
2.5×10^9	274.9	0.079	274.4	0.07892

[a] Simulation parameters: $\Lambda = \infty$; $D_A = D_B = 10^{-5}$ cm^2·s^{-1}; $E_{start} = E^0 + 0.500$ V; $(K_3\lambda^{1/2})^{-1} = 10$; $N = 20$, $\beta = 1.0$.

For species with different diffusion coefficients and with a reversible preceding reaction, Eq. (11) becomes

$$k_3^* + k_{-3}^* = (k_3 + k_{-3})\tau \leqslant \left[\frac{e^{N\beta} - 1}{30(e^{\beta} - 1)}\right]^2 (D_{min}/D_{max}) \quad (27)$$

After appropriate rearrangement of Eq. (27), one obtains

$$N \geqslant \ln\left[30(e^{\beta} - 1)\sqrt{(k_3 + k_{-3})\tau D_{max}/D_{min}} + 1\right]/\beta \quad (28)$$

At the same time, Eq. (8) requires that the following relationship must hold

$$N \geqslant \ln\left[(e^{10\beta} - 1)\sqrt{D_{max}/D_{min}} + 1\right]/\beta \quad (29)$$

Eq. (28) is the requirement of reaction layer, and correspondingly Eq. (29) is the request of diffusion layer for the grids number. For an accurate simulation, both Eqs. (28) and (29) must be satisfied. Assuming $D_{min}/D_{max} = 10^{-8}$ and $\lambda = 2.5\times10^9$, Eq. (28) requires $N \geqslant 26$, while Eq. (29) requires $N \geqslant 19$. Therefore at least 26 simulation grids must be used to fulfill both Eqs. (28) and (29). Choosing parameters corresponding to the last row in Table 12, simulations were conducted for two cases with $D_A = D_C = 10^{-13}$ cm^2·s^{-1}, $D_B = 10^{-5}$ cm^2·s^{-1} and $D_A = D_C = 10^{-5}$ cm^2·s^{-1}, $D_B = 10^{-13}$ cm^2·s^{-1}. The results in Fig. 4 show that the simulated curves are almost converged for $N < 26$, while for $N < 26$ the simulated voltammetric currents have obviously smaller values. For $N = 26$, the simulated cathodic peak current function is 0.0789 (literature value is 0.079), and the half peak potential $E_{p/2}$ is -0.0379 mV [literature value is $-0.2749 + (RT/2F)\ln(D_B/D_A) = -0.0383$ V]. For the case with $D_A = D_C = 10^{-5}$ cm^2·s^{-1} and $D_B = 10^{-13}$ cm^2·s^{-1}, the simulated voltammetric curves began to overlap when $N \geqslant 19$, which seems to contradict the prediction based on Eqs. (28) and (29). The reason is that B did not join the chemical reaction, so the thickness of the reaction layer should be calculated based on the diffusion coefficients of A and C. Since $D_A = D_C = D_{max}$, the reaction layer requires 17 grids, while the diffusion layer needs 19 simulation grids. The peak current function and half peak potential are 0.0789 (literature value is 0.079) and -0.5111 mV [literature value is $-0.2749 + (RT/2F)\ln(D_B/D_A) = -0.5115$ mV], in agreement with the literature values. In addition, the CE_i process that has an irreversible electron-transfer is also simulated, and the results in Table 13 also agree well with the literature results.[21]

EC_{cat} *case*

Based on Eqs. (28) and (29), it was known that the minimum value of N_{min} used should be 8 and 15 for $k_f^{\neq} = 10^2$ and 10^8, $\beta = 1.0$ and $\tau = 1$ s. From Table 14, the good consistency between the simulated results and those obtained by numerical resolutions can be noticed. In addition, increasing N could improve the simulation accuracy further. In addition, the simulation accuracy seems to be independent with the potential increment, and the calculation time is only dependent on the number of the simulation spatial grids and the potential increment, not on the value of the catalytic rate constant. The independence of simulation accuracy on the potential increment shows a significant advancement in comparison with other algorithms with stiff stability such as quasi-explicit and single alternating group explicit finite difference methods.[25,26] These

Table 13 Simulated voltammetric peak current functions and half-peak potentials for a reversible chemical reaction preceding an irreversible heterogeneous electron transfer[a]

$(K_3\lambda_i^{1/2})^{-1}$	N.S.		$\beta = 0.5$		$\beta = 1.0$	
	$E_{p/2}'$[a] (mV)	Ψ_{CE}[b]	$E_{p/2}'$ (mV)	Ψ_{CE}	$E_{p/2}'$ (mV)	Ψ_{CE}
0.2	44.2	0.444	44.5	0.4451	44.6	0.4451
1	51.4	0.318	51.4	0.3188	51.4	0.3189
10	82.2	0.080	82.4	0.0800	82.5	0.0801

[a] Simulation parameters: $\alpha = 0.5$; $D_A = D_B = 10^{-5}$ cm^2·s^{-1}; $E_{start} = E^0 + 0.3$ V; $\lambda_i = (k_3 + k_{-3})/b = 18$; $N = 10$ for $\beta = 1.0$ or $N = 15$ for $\beta = 0.5$. [b] $E_{p/2}' = (E_{p/2} - E^0)\alpha - RT/F \ln[K_3/(1 + K_3)] + RT/F \ln(\pi D_A b)^{1/2}/k_s$, where $b = \alpha Fv/(RT)$. [c] $\Psi_{CE} = i/FAc^*(D_A b)^{1/2}$, where c^* is the sum of the equilibrium concentrations of species A and C.

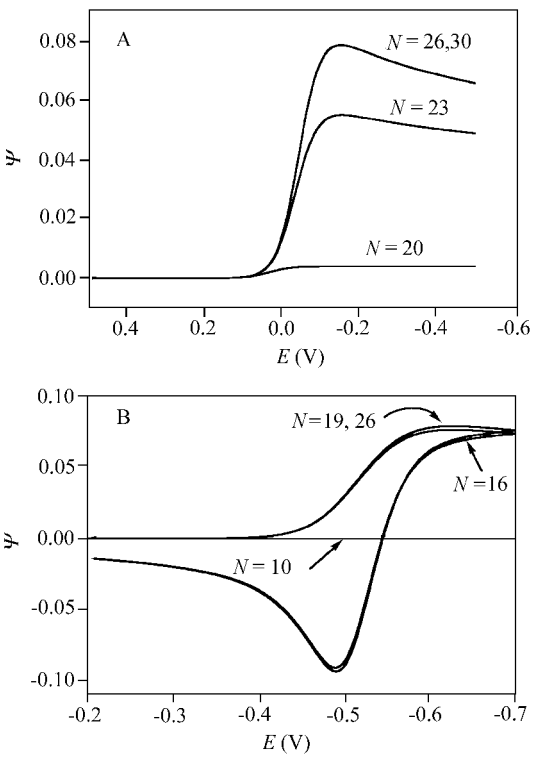

Fig. 4 Simulated voltammetric curves for a CE process with different number of simulation boxes as indicated on the corresponding curves. Simulation parameters are the same as the last row of Table 11 with the following exceptions: (A) $D_A = D_C = 10^{-13}$ cm^2·s^{-1}, $D_B = 10^{-5}$ cm^2·s^{-1} and (B) $D_A = D_C = 10^{-5}$ cm^2·s^{-1}, $D_B = 10^{-13}$ cm^2·s^{-1}.

features also parallel the fast implicit finite difference (FIFD) approach and have evidenced the very high simulation efficiency of EEGNA.

Based on logarithm analysis ($\ln[(\Psi_p - \Psi)/\Psi]$ vs. E plot) of the last row data in Table 14, Nernst factor (RT/F) and half-wave potential ($E_{1/2}$) could be estimated to be 25.69 mV (theoretical value: 25.69 mV) and 0.005 mV (theoretical value: 0 mV) respectively for $\Delta E = 1$ mV, while for $\Delta E = 5$ mV these values are 25.70 mV and 0.003 mV correspondingly. The good consistency with theoretical values further proves the simulation accuracy of EEGNA for such a stiff system.

Table 14 Simulated voltammetric peak current functions (Ψ_p) and relative CPU time (f_t) for a reversible electron transfer followed by an irreversible first-order catalytic chemical reaction[a]

$k_1^{\neq} = k_1/a$	N	$\Delta E = 5$ mV		$\Delta E = 1$ mV	
		Ψ_p	f_t	Ψ_p	f_t
		10.000[b]		10.000[b]	
10^2	6	8.955	1	8.955	4.4
	8	9.982	1.3	9.982	5.3
	10	10.000	1.4	10.000	5.8
		10000[b]		10000[b]	
10^8	10	904.2	1.4	904.2	5.8
	15	9987	2.0	9987	8.2
	20	10001	2.5	10001	9.8

[a] Simulation parameters: $E_{start} = E_0 + 0.200$ V; $E_{start} - E_{switch} = 0.500$ V; $D_A = D_B = 10^{-5}$ cm^2·s^{-1}; $a = 38.92$ s^{-1}; $\beta = 1.0$. [b] Obtained by numerical integration as reported in Ref. 24.

The efficiency of EEGNA in simulation of a stiff catalytic mechanism can be further demonstrated through checking the convergences of the simulated currents with the gradually increased network grid numbers in the cases of both EEGNA and UGNA. As seen from Fig. 5, the simulated current function increases to the final accurate

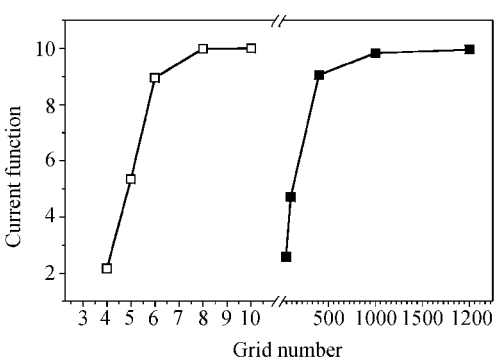

Fig. 5 Convergence of simulated voltammetric current with the increase of grid numbers used for exponentially expanded grid and uniform grid network approaches. Simulation parameters: $E_{start} = E_0 + 0.200$ V; $E_{start} - E_{switch} = 0.500$ V; $D_A = D_B = 10^{-5}$ cm^2·s^{-1}; $a = 38.92$ s^{-1}; $\beta = 1.0$ and $k_1^{\neq} = k_1/a = 10^2$. Open squares: EEGNA, solid squares: UGNA.

value (10.000) for EEGNA after the grid number is greater than 10. However, for UGNA, the simulated dimensionless current function only reaches 4.712 when the grid number is 100, and 9.956 even if the grid number has been increased to 2000. Therefore, the EEGNA has an incomparable simulation efficiency with respect to UGNA even for relatively small catalytic rate constant ($k_f^{\neq} = 10^2$). For $k_f^{\neq} = 10^8$, EEGNA only needs 15—20 grids to get a very accurate simulation, but UGNA has become impractical due to incredibly long computation time as well as large memory usage.

Conclusions

An exponentially expanded network model has been introduced for the network simulation of various electrochemical problems with one-dimensional diffusion geometry. E, CE, EC and EC_{cat} schemes have been considered as four typical cases in the context of the kinetic aspect of molecular electrochemistry. The exponentially expanded network method has been demonstrated to be competitive as a fast and accurate way for the simulation of stiff electrochemical problems with respect to uniform or quasi-uniform grid network approach as well as various explicit or quasi-explicit finite difference algorithms. In addition, the exponentially expanded network approach also has the ability to cope with systems with extremely widely dispersed diffusion coefficients, and bears an advantage of mathematical simplicity compared with other simulation techniques. All these features make it especially promising as a candidate for the construction of a general-purpose electrochemical simulator dealing with extremely complex electrochemical systems in the easiest and most convenient way.

References

1 Horno, J.; Gonzalezfernandez, C. F.; Hayas, A.; Gonzalezcaballero, F. *J. Membr. Sci.* **1989**, *42*, 1.

2 White, J. C. *Bull. Math. Biol.* **1986**, *48*, 353.

3 Wyatt, J. L.; Mikulecky, D. C.; De Simone, J. A. *Chem. Eng. Sci.* **1980**, *35*, 2115.

4 Mikulecky, D. C. *Comput. Chem.* **2001**, *25*, 369.

5 Horno, J.; García-Hernández, M. T. *J. Electroanal. Chem.* **1993**, *352*, 83.

6 Lopez-Garcia, J. J.; Horno, J.; Grosse, C. *J. Colloid Interface Sci.* **2002**, *251*, 85.

7 Moya, A. A; Horno, J. *J. Membr. Sci.* **2001**, *194*, 103.

8 Lopez-Garcia, J. J.; Horno, J.; Grosse, C. *Phys. Chem. Chem. Phys.* **2001**, *3*, 3754.

9 Moya, A. A.; Horno, J. *J. Phys. Chem. B* **1999**, *103*, 10791.

10 Moya, A. A.; Horno, J. J. *Electroanal. Chem.* **1998**, *459*, 145.

11 Moya, A. A.; Hayas, A.; Horno, J. *Electrochim. Acta* **1998**, *43*, 487.

12 Horno, J.; Garcia-Hernandez, M. T.; Castilla, J.; Gonzalez-Fernandez C. F. *Electroanalysis* **1996**, *8*, 1145.

13 Moya, A. A.; Hayas, A.; Horno, J. *Solid State Ionics* **2000**, *130*, 9.

14 González-Fernández, C. F.; García-Hernández, M. T.; Horno, J. *J. Electroanal. Chem.* **1995**, *395*, 39.

15 García-Hernández, M. T.; Castilla, J.; Gonzátez-Fernández, C. F.; Horno, J. *J. Electroanal. Chem.* **1997**, *424*, 207.

16 Deng, Z. X.; Lin, X. Q. *Chin. J. Anal. Chem.* **2000**, *28*, 930 (in Chinese).

17 Deng, Z. X.; Lin, X. Q. *Chin. J. Anal. Chem.* **1999**, *27*, 1376 (in Chinese).

18 Rudolph, M. *J. Electroanal. Chem.* **1991**, *314*, 13.

19 Fu, X. C.; Shen, W. X.; Yao, T. Y. *Physical Chemistry* (II), China High Education Press, Beijing, **1993** (in Chinese).

20 Bard, A. J.; Faulkner, L. R. *Electrochemical Methods: Fundamentals and Applications*, Wiley, New York, **1980**.

21 Nicholson, R. S.; Shain, I. *Anal. Chem.* **1964**, *36*, 706.

22 Andrieux, C. P.; Garreau, D.; Hapiot, P.; Savéant, J.-M. *J. Electroanal. Chem.* **1988**, *243*, 321.

23 Olmstead, M. L.; Hamilton, R. G.; Nicholson, R. S. *Anal. Chem.* **1969**, *41*, 260.

24 Rudolph, M. *J. Electroanal. Chem.* **1990**, *292*, 1.

25 Feldberg, S. W. *J. Electroanal. Chem.* **1990**, *290*, 49.

26 Deng, Z. X.; Lin, X. Q. *Chin. J. Chem.* **2002**, *20*, 252.

(E0209175 LI, L. T.; LING, J.)